Wasit Journal for Pure Science

Journal Homepage: https://wjps.uowasit.edu.iq/index.php/wjps/index
e-ISSN: 2790-5241 p-ISSN: 2790-5233

Study the Effect of Suction-Injection parameters Numerically and Analytically for Magneto hydrodynamic Jeffery Hamel Fluid Flow Problem

Ahmed Rasheed.Khlefha[1], Abeer Majeed Jasim[2]*

[1]Department of Mathematics, Faculty of Education, University of Sumer, Thi-Qar, IRAQ

[2]Department of Mathematics, Faculty of Science, University of Basrah, Basrah, IRAQ

* Corresponding Author: Ahmed Rasheed Khlefha

DOI: https://doi.org/10.31185/wjps.359
Received 03 March 2024; Accepted 10 May 2024; Available online 30 Jun 2024

ABSTRACT: This paper processes numerically and analytically the magnetohydrodynamic flow among two porous solid plate intersections at an angle or through non-parallel porous walls, which can be interpreted as a mix of Jeffery Hamel fluid flow additives from suction-injection parameters. In fluid mechanics, the equations of governing, which are transferred to the non-linear ordinary differential equation of third order, are modeled instead of the conventional Navier-Stokes equations by Maxwell's electromagnetism. In this study, the results obtained from the differential transform method ($\mathcal{DTM}$) and the numerical method BVP4c are compared to the results obtained from the optimal methods ($\mathcal{ODTM}$), which include the collocation differential transform method ($\mathcal{CDTM}$), the subdomain differential transform method ($\mathcal{SDTM}$), the least squares differential transform method ($\mathcal{LDTM}$), and the Galerkin differential transform method ($\mathcal{GDTM}$) A comparison is made between the approximate analytical and numerical solutions for different parameters like open angles (ε), Reynolds numbers (Re), injection parameters (S), and Hartmann numbers (Ha). The results demonstrate that the two approaches are very similar.

Keywords: Jeffery-Hemal, Fluid FloW, The Differential transform Method, MHD Flow.

1. INTRODUCTION

The Jeffery Hamel problem is a mathematical term for incompressible viscous fluid flow among non-parallel walls for convergent diverging channels, which Jeffery feigns [1] and Hamel [2]. This type of flow was first created by pioneers, who managed to make it famous by elevating it to a key position in the study of flow dynamics and establishing a solid mathematical formula for various mechanical circumstances. The numerous applications in biomedical engineering for MHD generators can be summarized as in Fig.1:

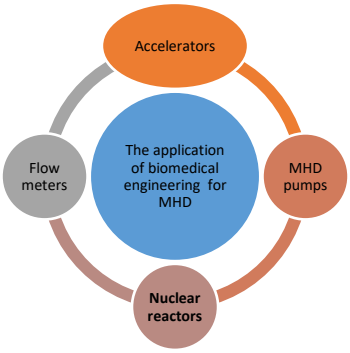

FIGURE 1. The Applications of MHD

*Corresponding author: arkdsh85@gmail.com

Since they are used in many industrial and natural environments and are considered useful in daily life and work, many scientists have been interested in this field in recent years [3-6]. Magneto-hydrodynamics has been the focus of many researchers [7-10]. In contrast, the flow of magnetic hydrodynamic nature is considered about the current induced in fluid moving in the presence of a magnetic field. The damping and control of electrically conductive fluids can be achieved by electromagnetic body force which is why the study of such flow is so interesting and has different applications in a variety of fields of technology and engineering. For example, Asghar et al [11] examined the boundary stresses stipulated in the tractive boundary condition on an incompressible magnetic hydrodynamic flow from Jeffrey Hamel for a viscous fluid. Dinarvand et al [12] analyzed the converging-diverging channel heat transfer and flow with the multiple slips effect which is a development of the Jeffery Hamel problem utilizing the mass-based hybrid nanofluid algorithm. Nadeem et al [13] investigated how mass and heat transfer affected blood flow through a stenosed, tapered porous artery using Newtonian bio-magnetic fluid. Chutia [14] looked into how an inclined magnetic field and variable thermal conductivity affected MHD plane poiseuille flow in a porous channel with a non-uniform plate temperature. Jasim [15] used the derivative series algorithm to investigate the non-slip and slip of unsteady flow fluid. Jasim [16] Studied the effect of MHD on squeezing flow of water-based Casson nanofluid in a porous medium between two parallel plates. Many researchers have been keenly interested in different analytical methods for studying fluid flow problems [17-28]. This research utilizes a significant method, called Differential Transformation, to address extremely nonlinear situations. This approach is specifically applied to evaluate ordinary differential equations [29,30]. The main objective of this work is to investigate the behavior of an unstable Magneto hydrodynamic fluid flow in divergent/convergent channels. $\mathcal{DTM}$ is a type of analytical approach for discovering approximate analytical solutions to nonlinear equations that cannot be solved exactly. It may be used to explain, forecast, and describe occurrences in systems induced by nonlinear processes. This analytical approach has been successful in solving the problem of fluid flow, producing the approximate- analytical solutions for the velocity, and studying differential equations governing the MHD Jeffery Hamel fluid flow. The impacts of the Reynolds number, Hartmann number, angle open, and injection-suction parameters on velocity profiles are graphically discussed.This article introduces a new approximation method called the optimal differential transform method. This method combines several techniques, including $\mathcal{DTM}, \mathcal{CDTM}, \mathcal{SDTM}, \mathcal{LDTM}$ and $\mathcal{GDTM}$.The primary characteristic of the $\mathcal{ODTM}$ strategy is its ability to rapidly converge while minimizing computational expenses. In order to validate the outcomes achieved by the $\mathcal{ODTM}$, the identical problems were additionally examined utilizing both the $\mathcal{DTM}$ and the numerical methodology. $\mathcal{BVP}4c$. The remaining sections are organized as follows: section two presents the statement of equations, section three discusses the ideal basis of $\mathcal{DTM}$ for ordinary differential equations, section four explores the application of $\mathcal{DTM}$ and $\mathcal{BVP}4c$, section five focuses on improving the analytical aspect, section six presents the convergence test, and section seven provides the results and discussion. Section eight contains the conclusion.

2. THE STATEMENT OF EQUATIONS

Two-dimensional and incompressible conducting viscous of fluid flow of two rigid plane walls which are in the intersection state from a source or sink with an angle of 2ε. geometric interpretation of physical phenomena that can be represented in the language of mathematics in the form of a model with physical parameters as depicted in Fig.2. The velocity $(\bar{u}_{\bar{r}}(\bar{r},\bar{\theta}),0)$ is depend on $\bar{r}$ and $\bar{\theta}$ [31,32] and only along a radial direction. The polar coordinates that represent this model using the momentum equations and the continuity equation, which are the Navier-Stokes equation, in the following form can be written as:

$$\frac{1}{\bar{r}}\frac{1}{\partial\bar{r}}\left(\bar{r}(\bar{u}_{\bar{r}}(\bar{r},\bar{\theta})-\psi si\,n\,\bar{\theta})\right)+\frac{1}{\bar{r}}\frac{1}{\partial\bar{\theta}}(\psi co\,s\,\bar{\theta})\;=0, \tag{1}$$

$$\frac{(\bar{u}_{\bar{r}}(\bar{r},\bar{\theta})-\psi\sin\bar{\theta})\left(\partial\bar{u}_{\bar{r}}(\bar{r},\bar{\theta})\right)}{\partial r}+\frac{(\psi\cos\bar{\theta})}{\bar{r}}\frac{\partial(\bar{u}_{\bar{r}}(\bar{r},\bar{\theta})-\psi\sin\bar{\theta})}{\partial\bar{\theta}}-\frac{(\psi\cos\bar{\theta})^2}{\bar{r}}=-\frac{1}{\rho}\;\frac{\partial p}{\partial\bar{r}}+\psi(\frac{\partial^2(\bar{u}_{\bar{r}}(\bar{r},\bar{\theta})-\psi\sin\bar{\theta})}{\partial\bar{r}^2}+$$

$$+\frac{1}{\bar{r}^2}\frac{\partial^2(\bar{u}_{\bar{r}}(\bar{r},\bar{\theta})-\psi\sin\bar{\theta})}{\partial\bar{\theta}^2}-\frac{(\bar{u}_{\bar{r}}(\bar{r},\bar{\theta})-\psi\sin\bar{\theta})}{\bar{r}^2}-\frac{2\partial(\psi\cos\bar{\theta})}{\bar{r}^2\partial\bar{\theta}})-\frac{\sigma B_0}{\rho\bar{r}^2}(\bar{u}_{\bar{r}}-\psi\sin\bar{\theta}), \tag{2}$$

$$(\bar{u}_{\bar{r}}(\bar{r},\bar{\theta})-\psi\sin\bar{\theta})\frac{\partial(\psi\cos\bar{\theta})}{\partial\bar{r}}+\frac{(\psi\cos\bar{\theta})}{\bar{r}}\frac{\partial(\psi\cos\bar{\theta})}{\partial\varphi}-\frac{(\psi\cos\bar{\theta})}{\bar{r}}(\bar{u}_{\bar{r}}(\bar{r},\bar{\theta})-\psi\sin\bar{\theta})==-\frac{1}{\rho\bar{r}}\;\frac{\partial p}{\partial\bar{\varphi}}+$$

$$\psi\left(\frac{\partial^2(\psi\cos\bar{\theta})}{\partial\bar{\theta}^2}\;+\frac{(\psi\cos\bar{\theta})}{\bar{r}^2}+\frac{2}{\bar{r}^2}\frac{\partial(\bar{u}_{\bar{r}}(\bar{r},\bar{\theta})-\psi\sin\bar{\theta})}{\partial\bar{\theta}}\right) \tag{3}$$

The flow can be described from the line source purely radial. Therefore, assume that $\bar{u}_{\bar{r}}=\bar{u}_{\bar{r}}(\bar{r},\bar{\theta})$ with using Eq.1as follows:

$$\bar{u}_{\bar{r}}=2\,\psi\sin\bar{\theta}+\frac{\mathcal{y}(\bar{\theta})}{\bar{r}}, \tag{4}$$

all derivatives are calculated with respect to $\mathcal{y}$ and substituting Eq. 4 in Eq.2 and Eq.3, yield

$$\left(\frac{y}{\bar{r}}+\psi\sin\bar{\theta}\right)\left(\frac{-y}{\bar{r}^2}\right)+\frac{(\psi\cos\bar{\theta})}{r}\left(\psi\cos\bar{\theta}+\frac{1}{\bar{r}}\frac{dy(\xi)}{d\xi}\right)-\frac{(\psi\cos\bar{\theta})^2}{\bar{r}}=\frac{1}{\rho}\frac{\partial p}{\partial\bar{r}}+\left(\frac{2y}{r^3}+\frac{1}{r}\left(\frac{-y}{\bar{r}^2}\right)+\frac{1}{\bar{r}^2}\bar{u}_{\bar{r}}\left(\frac{1}{\bar{r}}\frac{d^2y(\xi)}{d\xi^2}-\psi\sin\bar{\theta}\right)-\left(\frac{y}{\bar{r}^3}+\frac{\psi\sin\bar{\theta}}{\bar{r}^2}\right)+\frac{2}{\bar{r}^2}\psi\sin\bar{\theta}\right)-\frac{\sigma B_0}{\rho\bar{r}^2}\left(\frac{1}{\bar{r}}\frac{dy(\xi)}{d\xi}\psi\sin\bar{\theta}\right), \quad (5)$$

$$-\frac{(\psi\cos\bar{\theta})}{\bar{r}}\psi\sin\bar{\theta}+\frac{(\psi\cos\bar{\theta})}{r}\left(\frac{y}{\bar{r}}+\psi\sin\bar{\theta}\right)=\frac{1}{\rho\bar{r}}\frac{\partial p}{\partial\bar{\theta}}\left(\frac{\psi\cos\bar{\theta}}{\bar{r}^2}-\frac{\psi\cos\bar{\theta}}{\bar{r}^2}+\frac{2y}{\bar{r}^3}+\frac{2\psi\cos\bar{\theta}}{\bar{r}^2}\right), \quad (6)$$

after simplification, the Eq.5 and Eq. 6 can be formulated as follows:

$$\frac{1}{\rho}\frac{\partial p}{\partial r}=\frac{y^2}{\bar{r}^3}+\frac{y}{\bar{r}^2}\psi\sin\bar{\theta}-\frac{1}{\bar{r}^2}\frac{dy(\xi)}{d\xi}\psi\cos\bar{\theta}+\psi\frac{1}{\bar{r}^3}\frac{d^2y(\xi)}{d\xi^2}-\frac{\sigma B_0}{\rho\bar{r}^2}\left(\frac{1}{\bar{r}}\frac{dy(\xi)}{d\xi}+\psi\sin\bar{\theta}\right), \quad (7)$$

$$\frac{1}{\rho}\frac{\partial p}{\partial\bar{\theta}}=-\frac{y}{\bar{r}}\psi\cos\bar{\theta}+\psi\frac{2}{\bar{r}^2}\frac{dy(\xi)}{d\xi}, \quad (8)$$

Derivation Eq. 7 with respect to $\bar{\theta}$, Eq. 8 with respect to $\bar{r}$, become

$$\frac{1}{\rho}\frac{\partial^2 p}{\partial\bar{r}\partial\bar{\theta}}=\frac{2y}{r^3}\frac{dy(\xi)}{d\xi}+\frac{1}{\bar{r}^2}\frac{dy(\xi)}{d\xi}\psi\sin\bar{\theta}+\frac{y}{\bar{r}^2}\psi\cos\bar{\theta}-\frac{1}{\bar{r}^3}\frac{d^2y(\xi)}{d\xi^2}\psi\cos\bar{\theta}+\frac{1}{\bar{r}^2}\frac{dy(\xi)}{d\xi}\psi\sin\bar{\theta}+\frac{\psi}{\bar{r}^3}\frac{d^3y(\xi)}{d\xi^3}-\frac{\sigma B_\circ^2}{\rho\bar{r}^2}\left(\frac{1}{\bar{r}}\frac{dy(\xi)}{d\xi}+\psi\cos\bar{\theta}\right) \quad (9)$$

$$\frac{1}{\rho}\frac{\partial^2 p}{\partial r\partial\bar{\varphi}}=\frac{y}{\bar{r}^2}\psi\cos\bar{\theta}-\psi\left(\frac{4}{\bar{r}^3}\frac{dy(\xi)}{d\xi}\right), \quad (10)$$

subtract the last two equations, the result is:

$$\frac{d^3y(\xi)}{d\xi^3}+\frac{2y}{\psi}\frac{dy(\xi)}{d\xi}+\frac{4}{\psi}\frac{dy(\xi)}{d\xi}\psi\sin\bar{\theta}-\frac{1}{\psi}\frac{d^2y(\xi)}{d\xi^2}\psi\cos\bar{\theta}+4\frac{dy(\xi)}{d\xi}-\frac{\sigma B_0^2}{\rho\psi}\left(\frac{dy(\xi)}{d\xi}+\psi\bar{r}\cos\bar{\theta}\right)=0, \quad (11)$$

Eq.9 is normalizing of the velocity distribution at $\bar{\theta}=0$. The non-dimensional variables can be introduced as follows:

$$Y(\xi)=\frac{y(\bar{\theta})}{y(0)},\qquad \xi=\frac{\bar{\theta}}{\varepsilon},\qquad \delta=\frac{\psi}{y(0)}, \quad (12)$$

Eq.13 and Eq. 11 are given the following equation

$$\frac{d^3Y(\xi)}{d\xi^3}+\frac{2\varepsilon^2y(0)}{\psi}\frac{dY(\xi)}{d\xi}+\frac{2\varepsilon^2\bar{r}}{\psi}\frac{dY(\xi)}{d\xi}\psi\sin(\varepsilon\xi)-\frac{\varepsilon}{\psi}\frac{d^2Y(\xi)}{d\xi^2}\bar{r}\psi\cos(\varepsilon\xi)+4\varepsilon^2\frac{dY(\xi)}{d\xi}-\frac{\sigma{B_0}^2}{\rho\psi}\left(\varepsilon^2\frac{dY(\xi)}{d\xi}+\frac{1}{y(0)}\psi\varepsilon^3\bar{r}\cos(\varepsilon\xi)\right)=0, \quad (13)$$

The final form of the mathematical model can be predicted after using non-dimensional transformations with a third-order nonlinear differential equation, which is

$$\frac{d^3Y(\xi)}{d\xi^3}-\varepsilon S\cos(\varepsilon\xi)\frac{d^2Y(\xi)}{d\xi^2}+2\varepsilon ReY\frac{dY(\xi)}{d\xi}+(2\varepsilon S\sin(\varepsilon\xi)+4\varepsilon^2-Ha\,\varepsilon^2)\frac{dY(\xi)}{d\xi}-\frac{HaS}{Re}\varepsilon^3\cos(\varepsilon\xi)=0, \quad (14)$$

The groups of boundary conditions and initial are:

$$Y(1)=0, Y(0)=1,\ \frac{dY(0)}{d\xi}=0, \quad (15)$$

There are two cases in which channels can be described:

- The channel of divergent: $\varepsilon>0,\ y_{max}>0,$
- The channel of convergent: $\varepsilon<0,\ y_{max}<0,$

Thus, the definition of the Hartmann parameter is $Ha=\frac{\sigma{B_0}^2}{\rho\psi}$, the Reynolds parameter is $Re=\frac{y(0)\varepsilon}{\psi}$ and the suction- injection parameter is $S=\frac{\delta\bar{r}\varepsilon}{\psi}$ where ψ is the kinematic viscosity, $\bar{r}$ is the length and δ is injection velocity for the fluid. In addition, S denoted the ratio of inertial to viscous forces can be divided as follows:

- injection parameter: $S<0,$
- impermeability: $S=0,$
- Suction parameter: $S>0.$

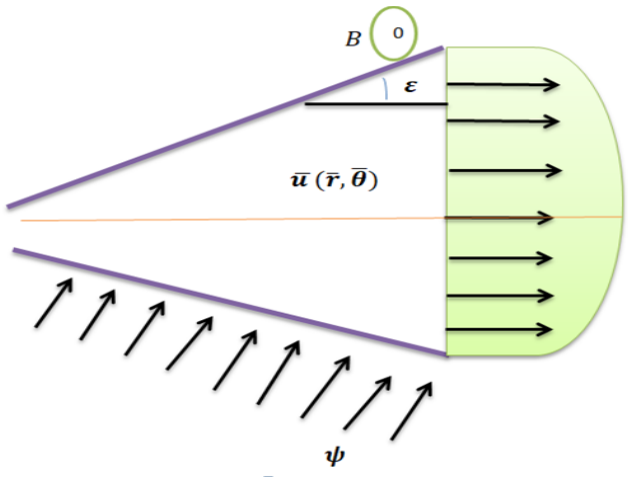

Figure 2. The Designation of Problem

3. THE OPTIMAL FUNDAMENTAL DIFFERENTIAL TRANSFORM SCHEME FOR ORDINARY DIFFERENTIAL EQUATIONS

Obtaining approximate- analytical solution for some of different fluid flow problem. Consequently, in this section we will display the basic rules of one of the semi- analytical methods which we have adopted in finding these solutions, namely differential transform scheme which was first introduced by Zhou in (1986). The DTS is an iterative scheme based on the utilize of the Taylor series expansion of differential equations. The differential transformation of a function $\mathcal{Y}(\xi)$ of the $\bar{k}$th derivative is introduce as:

$$\mathcal{W}(\bar{k}) = \frac{1}{\bar{k}!}\left(\frac{d^{\bar{k}}y(\xi)}{d\xi^{\bar{k}}}\right)_{\xi=\xi_0}, \quad (16)$$

Where $\mathcal{W}(\bar{k})$ is the transformed function and $\mathcal{Y}(\xi)$ is original function. The inverse transform for the function $\mathcal{W}(\bar{k})$ gives the n-terms approximation solution can be written as the following:

$$\mathcal{Y}(\xi) = \sum_{\bar{k}=0}^{n} \mathcal{W}(\bar{k})(\xi - \xi_0)^{\bar{k}}, \quad (17)$$

Substituting equation (16) into equation (17), gives

$$\mathcal{Y}(\xi) = \sum_{\bar{k}=0}^{n} \frac{(\xi-\xi_0)^{\bar{k}}}{\bar{k}!}\left(\frac{d^{\bar{k}}y(\xi)}{d\xi^{\bar{k}}}\right)_{\xi=\xi_0}, \quad (18)$$

Now, if $t(\xi)$ and $v(\xi)$ are two functions of ξ and $T(\bar{k})$and $V(\bar{k})$ are the transformed functions corresponding to $t(\xi)$ and $v(\xi)$, The basic arithmetic operations that are performed by differential transformation and are explained in Table 1 as follows:

Table 1: The functions of differential Transformation

	Basic function	Changed function
1	$\mathcal{Y} = t(\xi) \pm v(\xi)$	$\mathcal{W}(\bar{k}) = \ddot{\mathcal{T}}(\bar{k}) \pm \ddot{\mathcal{V}}(\bar{k})$
2	$\mathcal{Y}(\xi) = ct(\xi)$	$\mathcal{W}(\bar{k}) = c\ddot{\mathcal{T}}(\bar{k})$
3	$\mathcal{Y}(\xi) = t(\xi)v(\xi)$	$\mathcal{W}(\bar{k}) = \sum_{i=0}^{\bar{k}} \ddot{\mathcal{T}}(i)\ddot{\mathcal{V}}(\bar{k}-i)$
4	$\mathcal{Y}(\xi) = \frac{d^n t(\xi)}{d\xi^n}$	$\frac{(\bar{k}+n)!}{\bar{k}!}\ddot{\mathcal{T}}(\bar{k}+n)$
5	$\mathcal{Y}(\xi) = \sin(z\xi + \tau)$	$\mathcal{W}(\xi) = \frac{z^k}{k!}\sin\left(\frac{\pi\bar{k}}{2} + \tau\right)$
6	$\mathcal{Y}(\xi) = \cos(\mathcal{Z}\xi + \tau)$	$\mathcal{W}(\xi) = \frac{z^k}{k!}\cos\left(\frac{\pi k}{2} + \tau\right)$

4. MAGNETO HYDRODYNAMIC JEFFERY HAMEL FLOW WITH SUCTION-INJECTION USING DTM AND BVP4C

In this section, two schemes $\mathcal{DTM}$ and BVP4c are implemented to solve magneto hydrodynamic Jeffery Hamel flow with suction-injection problem in order to obtain approximate analytical and numerical solutions respectively, which can be summarized as follows:

- **The analytical part**

According to the differential transform method and after utilizing the basic operations of differential transform scheme to Eq.16, we obtain the iterative scheme given as follows:

$$(\bar{k}+1)(\bar{k}+2)(\bar{k}+3)\mathcal{W}(\bar{k}+3) = \varepsilon S\sum_{i=0}^{\bar{k}}\left(\varepsilon^{\bar{k}-i}\frac{cos\left(\pi\frac{\bar{k}-i}{2}\right)}{(\bar{k}-i)!}(i+1)(i+2)\mathcal{W}(i+2)\right)$$

$$-2\varepsilon\, Re\sum_{i=0}^{\bar{k}}\left((\bar{k}-i+1)\mathcal{W}(\bar{k}-i+1)\mathcal{W}(i)\right)-2\varepsilon\, S\sum_{i=0}^{\bar{k}}\left(\varepsilon^{\bar{k}-i}\frac{\sin\left(\pi\frac{\bar{k}-i}{2}\right)}{(\bar{k}-i)!}(i+1)\mathcal{W}(i+1)\right)$$

$$-4\varepsilon^2(\bar{k}+1)\mathcal{W}(\bar{k}+1)-\varepsilon^2\, Ha(\bar{k}+1)\mathcal{W}(\bar{k}+1)+\varepsilon^{\bar{k}+3}SHa\frac{\cos\left(\pi\frac{\bar{k}}{2}\right)}{Re\;\bar{k}!}, \qquad (19)$$

The boundary condition reduces to

$$\mathcal{W}(0)=1,\ \mathcal{W}(1)=0,\mathcal{W}(2)=\Pi \qquad (20)$$

where Π can be determined by using $\mathcal{Y}(1)=0$ with using the iterative formulas (19), yield

$$\mathcal{Y}_1(\xi)=1,$$

$$\mathcal{Y}_2(\xi)=1+\Pi\xi^2,$$

$$\mathcal{Y}_3(\xi)=1+\Pi\xi^2+\left(\frac{2\Pi S\varepsilon Re+\varepsilon^3 HaS}{6Re}\right)\xi^3,$$

$$\mathcal{Y}_4(\xi)=1+\Pi\xi^2+\left(\frac{2\Pi S\varepsilon Re+\varepsilon^3 HaS}{6Re}\right)\xi^3+\left(\frac{1}{24Re}(2\Pi\varepsilon^2S^2Re+Ha\varepsilon^4S^2)-\frac{1}{24}(2Ha\Pi\varepsilon^2+4\varepsilon\Pi Re-8\Pi\varepsilon^2)\right)\xi^4,$$

$$\mathcal{Y}_5(\xi)=1+\Pi\xi^2+\left(\frac{2\Pi S\varepsilon Re+\varepsilon^3 HaS}{6Re}\right)\xi^3+\left(\frac{1}{24Re}(2\Pi\varepsilon^2S^2Re+Ha\varepsilon^4S^2)-\frac{1}{24}(2Ha\Pi\varepsilon^2+4\varepsilon\Pi Re-\right.$$

$$\left.8\Pi\varepsilon^2)\right)\xi^4+\left(\left(\frac{Ha\varepsilon^4S^2-10\Pi\varepsilon^3S+2\Pi\varepsilon^3S^4Re-4\Pi\varepsilon^2ReS^2+2\Pi\,\varepsilon^3HaS^2}{120}\right)-\left(\frac{2\varepsilon^2\Pi SRe+HaS\varepsilon^3+2\Pi\varepsilon^4S}{60\varepsilon^2}\right)\right.$$

$$\left.+\left(\frac{6\Pi\varepsilon^3SHaRe-8\Pi\varepsilon^3SRe-4HaS\varepsilon^4Re+\varepsilon^5Ha^2SRe-\varepsilon^5HaS}{120Re}\right)\right)\xi^5,$$

⋮

The required approximate analytical solution is

$$\mathcal{Y}(\xi)=1+\Pi\xi^2+\left(\frac{2\Pi S\varepsilon Re+\varepsilon^3 HaS}{6Re}\right)\xi^3+\left(\frac{1}{24Re}(2\Pi\varepsilon^2S^2Re+Ha\varepsilon^4S^2)-\frac{1}{24}(2Ha\Pi\varepsilon^2+4\varepsilon\Pi Re-+8\Pi\varepsilon^2)\right)\xi^4$$

$$+\left(\left(\frac{Ha\varepsilon^4S^2-10\Pi\varepsilon^3S+2\Pi\varepsilon^3S^4Re-4\Pi\varepsilon^2ReS^2+2\Pi\,\varepsilon^3HaS^2}{120}\right)-\left(\frac{2\varepsilon^2\Pi SRe+HaS\varepsilon^3+2\Pi\varepsilon^4S}{60\varepsilon^2}\right)\right.$$

$$\left.+\left(\frac{6\Pi\varepsilon^3SHaRe-8\Pi\varepsilon^3SRe-4HaS\varepsilon^4Re+\varepsilon^5Ha^2SRe-\varepsilon^5HaS}{120Re}\right)\right)\xi^5+\cdots. \qquad (21)$$

- **The Numerical part**

The equation of nonlinear ordinary differential Eq.14 with boundary conditions are solved numerically by using BVP4c function technique by MATLAB. For finding the solution, the prerequisites are reducing a higher order initial assumptions for the new variables. Also, the transformed governing equation is reducing into equation of first order ordinary differential equation, some new variables were defined as

$$\mathcal{Y}(\xi)=\mathrm{G}_1,\ \frac{d\mathcal{Y}(\xi)}{d\xi}=\mathrm{G}_2,\ \frac{d^2\mathcal{Y}(\xi)}{d\xi^2}=\mathrm{G}_3, \qquad (22)$$

$$\frac{d^3\mathcal{Y}(\xi)}{d\xi^3}=\varepsilon S\cos(\varepsilon\xi)\ \mathrm{G}_3-2\varepsilon Re\ \mathrm{G}_1\mathrm{G}_2-(2\varepsilon S\sin(\varepsilon\xi)+4\varepsilon^2-\varepsilon^2\, Ha)\mathrm{G}_2+\frac{\varepsilon^3 SHa}{Re}\cos(\varepsilon\xi). \qquad (23)$$

Hence, a coupled of first-order ordinary differential equations and new boundary conditions were created from the coupled higher order differential equation and its accompanying boundary conditions. The ordinary differential equations topic to the boundary and initial conditions:

$$\mathrm{G}_1(1)=0,\ \mathrm{G}_1(0)=1,\ \mathrm{G}_2(0)=0,$$

Eq .22 and Eq .23 having been numerically integrated to a predetermined end point as an initial value problem. All these simplifications were necessary in order to use the MATLAB packages. This program is run with a step size of 0.1 and then solved for the range of 0 to 1 and back again.

5. IMPROVE ANALYTICAL ASPECT

For bettering the estimated analytical solution derived from DTM in Equation (21) that incorporates $\xi,\xi^2,\xi^3,\xi^4,\xi^5,\xi^6,\xi^7,\xi^8,\xi^9,\xi^{10}$, suppose the estimated analytical solution takes the subsequent form:

$$\tilde{\mathcal{Y}}(\xi) = (1-\xi^2) + \Pi_1(\xi^2-\xi^3) + \Pi_2(\xi^2-\xi^4) + \Pi_3(\xi^2-\xi^3) + \Pi_4(\xi^2-\xi^4) + \Pi_5(\xi^2-\xi^5) + \Pi_6(\xi^2-\xi^6) + \Pi_7(\xi^2-\xi^7) + \Pi_8(\xi^2-\xi^8) + \Pi_9(\xi^2-\xi^9) + \Pi_{10}(\xi^2-\xi^{10}). \quad (24)$$

To determine the appropriate values for $\Pi_k, k = 1,2,4,\dots,10$, We utilize the weighted residual methods to obtain the optimal coefficients for ξ The Weighted Residuals approach, a numerical technique, was used to approximate solutions to differential equations. Let's examine the use of a differential operator D of a given function $\mathcal{Y}(\xi)$, which produces a new function $\tilde{f}$.

$$\mathcal{D}\big(\mathcal{Y}(\xi)\big) = \tilde{f}(\xi) . \quad (25)$$

The approximation of the $\mathcal{Y}$ variable is often accomplished by representing it as a linear combination of fundamental functions $\tilde{\mathcal{Y}}$ chosen from a linearly independent collection. This can be understood as,

$$\mathcal{Y} \cong \tilde{\mathcal{Y}} = \sum_{i=1}^{n} \Pi_i \tilde{\emptyset}_i . \quad (26)$$

Applying the difference operators $\mathcal{D}$ usually does not result in $\tilde{f}(\xi)$. Consequently, it is anticipated that an inaccuracy or residual will be present.

$$R(\xi) = \mathcal{D}\left(\tilde{\mathcal{Y}}(\xi)\right) - \tilde{f}(\xi) \neq 0. \quad (27)$$

The basic idea of weighted residual methods aims to achieve a zero residual throughout the entire domain by averaging. To put it differently:

$$\int_a^b \mathcal{R}(\xi)\, \tilde{w}_i d\xi, i = 1,2,\dots,n . \quad (28)$$

The total number of weight functions, shown as $\ddot{w}_i$ is the same as the number of unknown values in the function $\tilde{\mathcal{Y}}$, shown as Π_i. The outcome is a set of n algebraic formulas that describe the unknown constants Π_i. The parts that follow describe three different ways to use weighted residual methods.

5.1 – The Collocation Method

In this approach, the weighting functions are obtained by utilizing a collection of Dirac (δ) functions within the specified domain, specifically is $\ddot{w}_i = (\xi) = \delta(\xi - \xi_i)$.The Dirac delta function is precisely defined as

$$\ddot{w}_i = \delta(\xi - \xi_i) = \begin{cases} 1 & if\ \xi = \xi_i \\ 0 & \text{Otherwises} \end{cases} \quad (29)$$

The residual functions can be obtained by substituting Eq. (24) into Eq. (14), and denoted as $\mathcal{R}(\Pi_1, \Pi_2, \dots, \Pi_{10}, \xi)$ may be determined,

$$\mathcal{R}(\Pi_0, \Pi_1, \dots, \Pi_{10}) = 6\Pi_2 + 24\Pi_3\xi + 60\Pi_4\xi^2 + 120\Pi_5\xi^3 + 210\Pi_6\xi^4 + 336\Pi_7\xi^5 + 504\Pi_8\xi^6 + 720\Pi_9\xi^7 - S\varepsilon\cos(\varepsilon\xi)(-2 + \Pi_2(6\xi - 2) + \Pi_3(12\xi^2 - 2) + \Pi_4(20\xi^3 - 2) + \Pi_5(30\xi^4 - 2) + \Pi_6(42\xi^5 - 2) + \Pi_7(56\xi^6 - 2) + \Pi_8(72\xi^7 - 2) + \Pi_9(90\xi^8 - 2)) + 2\varepsilon R_a(1 - \xi^2 + \Pi_2(\xi^3 - \xi^2) + \Pi_3(\xi^4 - \xi^2) + \Pi_4(\xi^5 - \xi^2) + \Pi_5(\xi^6 - \xi^2) + \Pi_6(\xi^7 - \xi^2) + \Pi_7(\xi^8 - \xi^2) + \Pi_8(\xi^9 - \xi^2) + + \Pi_9(\xi^{10} - \xi^2))(-2\xi + \Pi_2(3\xi^2 - 2\xi) + \Pi_3(4\xi^3 - 2\xi) + \Pi_4(5\xi^4 - 2\xi) + \Pi_5(6\xi^5 - 2\xi) + \Pi_6(7\xi^6 - 2\xi) + \Pi_6(7\xi^6 - 2\xi) + \Pi_7(8\xi^7 - 2\xi) + \Pi_8(9\xi^8 - 2\xi) + \Pi_9(10\xi^9 - 2\xi)) + (2S\varepsilon\sin(\varepsilon\xi) + 4\varepsilon^2 - H_a\varepsilon^2) - 2\xi + \Pi_2(3\xi^2 - 2\xi) + \Pi_3(4\xi^3 - 2\xi) + \Pi_9(10\xi^9 - 2\xi)) + - \frac{H_a S\varepsilon^3\cos(\varepsilon\xi)}{R_a} \quad (30)$$

Nevertheless, the residual functions must approximate 0. To accomplish this goal, it is important to choose four unique positions inside the domain $\xi_i \in [0,1]$. Finally, by plugging in these points into the residual function, denoted as $\mathcal{R}(\Pi_1, \Pi_2, \dots, \Pi_{10}, \xi)$, a set of ten equations and ten unknown coefficients was obtained. After determining the unknown parameters $(\Pi_1, \Pi_2, \dots, \Pi_{10})$, they will be inserted into Equation (24) to get the approximation solution.

5.2 - The Sub-domain Collocation Method

This is an alternate approach that can be utilized to calculate the parameters $\Pi_i, 0,1,\dots,n$. The domain is divided into n sections.

$$\ddot{w}_i = \begin{cases} 1 & if\ \xi_i \le \xi \le \xi_{i+1} \\ 0 & \text{Otherwise} \end{cases}, \quad (31)$$

The objective of this strategy is to minimize the remaining error within each of the chosen subdomains. Therefore, equation (15) is satisfied in each subdomain, leading to a change of Eq. (30).

$$\int_a^b \ddot{w}_i R(\xi)\, d\xi = \int_{\xi_i}^{\xi_{i+1}} R(\xi)\, d\xi = 0 \text{ , for } i = 1,2,\dots.n \quad (32)$$

The trial function must adhere to the boundary condition stated in Equation (15) and can be as the function that's stated in Equation (24). The residual will be represented by Equation (30). By replacing the residual function, denoted as $\mathcal{R}(\Pi_0, \dots, \Pi_{10}, \xi)$, in equation (32), a system of four equations is obtained. By calculating this system of equations, one can derive the coefficients as follows $(\Pi_1, \dots, \Pi_{10})$. It is important to mention that the sub-domains might be freely selected. Under many circumstances, evenly partitioning the entire domain is the optimal choice. Nevertheless, choosing for an irregular selection might be more advantageous if a greater level of detail is required in a particular region.

5.3 – The Least Square Method

The reason for the name becomes clear when we consider the goal of reducing the total of squared residuals. To put it succinctly, at least of

$$\ddot{\mathcal{G}} = \int_a^b R(\xi)R(\xi)\,d\xi = \int_a^b R^2(\xi)\,d\xi. \quad (33)$$

In order to obtain the minimum value of this scalar function, it is necessary to equate each derivative of that function with respect to all the unknown variables to 0. To put it differently:

$$\frac{\partial \ddot{\mathcal{G}}}{\partial \Pi_i} = 2\int_a^b R(\xi)\frac{\partial R}{\partial \Pi_i}d\xi = 0. \quad (34)$$

Upon comparing with Equation (28), it is apparent that the weight functions exhibit the subsequent qualities:

$$\ddot{\mathrm{w}}_\iota = 2\frac{\partial \mathcal{R}}{\partial \Pi_i}, \quad (35)$$

However, the value of the coefficient of two can be excluded as it cancels out within the equation. Therefore, the weight functions used in the least-squares approach are equivalent to the derivatives of the residual with respect to the undefined values.

$$\ddot{\mathrm{w}}_\iota = \frac{\partial \mathcal{R}}{\partial \Pi_i}. \quad (36)$$

The trial function has to satisfy the boundary condition specified in Equation (15), and thus it will be considered as the function defined in Equation (24). The residual will be denoted by Equation (30). By substituting the residual function, represented as $\mathcal{R}(\Pi_1, \dots, \Pi_5, \xi)$, into Equation (34), a set of four equations may be derived. Resolving this set of equation will allow for the calculation of the values $(\Pi_1, \Pi_2 \dots, \Pi_1)$.

5.4 – The Galerkin Method

This approach may be regarded as a modification of the least-squares Approach (LSM). Instead of using the derivative of the residual to the unidentified variable Π_i, the derivatives of the approximate function or trial function are employed. Weight functions are used in this approach.

$$\ddot{\mathrm{w}}_\iota = \frac{\partial \ddot{\mathcal{J}}}{\partial \Pi_i}, i = 1,2, \dots, n. \quad (37)$$

To begin, let us examine the trial function, referred to as Eq. (24), which satisfies the specified boundary condition described in Eq. (15). The weight functions may be obtained by employing Equation (45), allowing for the establishment of a set of algebraic formulas. Afterwards, resolving this collection of equations results in the coefficients as follows $(\Pi_1, .., \Pi_{10})$. The approximate result can be obtained by inserting them into Equation (24).

6. CONVERGENCE

This section will go over the analytical approximation solutions that converge when $\mathcal{DTM}$ is applied to ordinary differential equations that are nonlinear. We will also look at how to derive the convergent condition to test the results that come out of this method, which are power series. To further understand how these results converge, we will be discussing some relevant theorems:

Theorem [33]: Let $\mathcal{P}$ be an operator from a Hilbert space $\mathcal{H}_0$ into $\mathcal{H}_0$ and let $\mathcal{W}$ be an exact solution of Equation (15) , then $\sum_{\bar{k}=0}^{\infty}\mathcal{W}(\bar{k})\xi^{\bar{k}}$ which is obtained by Equation. (17), converges to the exact solution, if there exists $0 \le \pi < 1$ such that $\|\mathcal{W}_{\bar{k}+1}\| \le \pi\|\mathcal{W}_{\bar{k}}\| \quad \forall \bar{k} \in \mathrm{N} \cup \{0\}$.

Proof: we have

$\widetilde{\Psi}_0 = 0$

$\widetilde{\Psi}_1 = \widetilde{\Psi}_0 + \mathcal{W}_1 = \mathcal{W}_1.$

$\widetilde{\Psi}_2 = \widetilde{\Psi}_1 + \mathcal{W}_2 = \mathcal{W}_1 + \mathcal{W}_2.$

$\vdots$

$\widetilde{\Psi}_{\mathrm{n}} = \widetilde{\Psi}_{\mathrm{n}-1} + \mathcal{W}_{\mathrm{n}} = \mathcal{W}_1 + \mathcal{W}_2 + \cdots + \mathcal{W}_{\mathrm{n}}.$

We will demonstrate that the sequence $\{\widetilde{\Psi}_{\mathrm{n}}\}_{n=0}^{\infty}$ is a Cauchy sequence in the Hilbert Space $\mathcal{H}_0$.

Now for

$$\left\|\widetilde{\Psi}_{\mathrm{n}+1} - \widetilde{\Psi}_{\mathrm{n}}\right\| = \|\mathcal{W}_{\mathrm{n}+1}\| \le \pi\|\mathcal{W}_{\mathrm{n}}\| \le \pi^2\|\mathcal{W}_{\mathrm{n}-1}\| + \cdots \le \pi^{\mathrm{n}}\|\mathcal{W}_0\|$$

For any natural numbers n and m, $n \ge m$ we have,

$$\left\|\widetilde{\Psi}_{\mathrm{n}} - \widetilde{\Psi}_{\mathrm{m}}\right\| = \left\|\left(\widetilde{\Psi}_{\mathrm{n}} - \widetilde{\Psi}_{\mathrm{n}-1}\right) + \left(\widetilde{\Psi}_{\mathrm{n}-1} - \widetilde{\Psi}_{\mathrm{n}-2}\right) + \cdots \left(\widetilde{\Psi}_{\mathrm{m}-2} - \widetilde{\Psi}_{\mathrm{m}+1}\right) + \left(\widetilde{\Psi}_{\mathrm{m}+1} - \widetilde{\Psi}_{\mathrm{m}}\right)\right\| \le \left\|\widetilde{\Psi}_{\mathrm{n}} - \widetilde{\Psi}_{\mathrm{n}-1}\right\|$$

$$+\left\|\widetilde{\Psi}_{\mathrm{n}-1} - \widetilde{\Psi}_{\mathrm{n}-2}\right\| + \cdots \left\|\widetilde{\Psi}_{\mathrm{m}-2} - \widetilde{\Psi}_{\mathrm{m}+1}\right\| + \left\|\widetilde{\Psi}_{\mathrm{m}+1} - \widetilde{\Psi}_{\mathrm{m}}\right\| \le \pi^{\mathrm{n}}\|\mathcal{W}_0\| + \pi^{\mathrm{n}-1}\|\mathcal{W}_0\| + \pi^{\mathrm{n}-2}\|\mathcal{W}_0\| +$$

$$+\pi^{\mathrm{n}-3}\|\mathcal{W}_0\| + \cdots + \pi^{\mathrm{m}+2}\|\mathcal{W}_0\| + \pi^{\mathrm{m}+1}\|\mathcal{W}_0\| \le (\pi^{\mathrm{m}+1} + \pi^{\mathrm{m}+2} + \cdots)\|\mathcal{W}_0\| = \frac{\pi^{\mathrm{m}+1}}{(1-\pi)}\|\mathcal{W}_0\|.$$

It may be inferred that $\lim_{n,m\to\infty} \|\widetilde{\Psi}_n - \widetilde{\Psi}_m\| = 0$, meaning $\{\widetilde{\Psi}_n\}_{n=0}^{\infty}$ is a Cauchy sequence in the Hilbert space $\mathcal{H}$ and it converges to $\widetilde{\Psi}$ for any $\widetilde{\Psi} \in \mathcal{H}$. From the theorem can be determined the convergence of $\mathcal{DTM}$ through introducing the convergence condition in the following definition and corollary.

Definition [34]: For every $j \in \mathrm{N} \cup \{0\}$, π_j can be defined as

$$\pi_j = \begin{cases} \dfrac{\|\mathcal{W}_{j+1}\|}{\|\mathcal{W}_j\|} & \|\mathcal{W}_j\| \neq 0 \\ 0 & \|\mathcal{W}_j\| = 0 \end{cases}.$$

Corollary [35]: If $0 \leq \pi_j < 1$, $j = 1.2, \ldots$, then $\sum_{k=0}^{\infty} \mathcal{W}_j$ is converges to the exact solution $\mathcal{W}$. To determine the convergence of the solutions, we can apply the convergence condition using the L_∞-norm. $\mathcal{DTM}$. Since $\pi_0 = \frac{\|\mathcal{W}_1\|}{\|\mathcal{W}_0\|} = 0 < 1$, $\pi_1 = \frac{\|\mathcal{W}_2\|}{\|\mathcal{W}_1\|} = 0 < 1$, $\pi_2 = \frac{\|\mathcal{W}_3\|}{\|\mathcal{W}_2\|} = 0 < 1$, ... In a similar manner, $\pi_j = 0$ for all j . All answers have been obtained for the result. therefore $\mathcal{Y}(\xi) = \sum_{k=0}^{\infty} \mathcal{W}(k)\xi^{\bar{k}}$ is convergent.

7. RESULTS AND DISCUSSION

A brief work of the influence of physical parameters such as $\varepsilon, S, \mathrm{Re}$ and Ha is discussed on the velocity profile $\mathcal{Y}(\xi)$.The comparison of the results for $\mathcal{DTM}, \mathcal{CDTM}, \mathcal{SDTM}, \mathcal{LDTM}$ and $\mathcal{GDTM}$ with the numerical results generated using the $\mathcal{BVP}4\mathrm{c}$ is provided in Tables 2–7. Also, the errors of percentage were derived in Tables 8-11, It is evident from these data that $\mathcal{CDTM}, \mathcal{SDTM}, \mathcal{LDTM}$ and $\mathcal{GDTM}$ all outperform $\mathcal{DTM}$ in terms of accuracy. The values of π demonstrate consistency to the decimal place and remain constant when the iterative techniques are expanded, as shown in Table 11. The results of these solutions can be represented graphically which is the impact of the dimensionless velocity $\mathcal{Y}(\xi)$ as shown in Figs. 3-10 for various parameters for both cases divergent and convergent channel. Fig. 3 and 4 show that it is important to note that, as the Hartman number rises, the velocity $\mathcal{Y}(\xi)$ increases for both convergent and divergent channels. The momentum that stabilizes the velocity profile is moving in the opposite direction of the Lorentz force effect. In Fig 5 and Fig 6 depicted the influence of the injection- suction parameter S. Because the radial component of the velocity δ and the radial velocity $\bar{u}_{\bar{r}}$ follow the same course in the diverging channel, the suction exerts an impact that favors the radial velocity, the suction has an effect that favors the radial velocity. However, in the case of convergent channels, Because the radial component of δ direction is opposite that of the flow radial velocity, the suction velocity responds in the opposite way, decreasing. The impact of the dimensionless velocity $\mathcal{Y}(\xi)$ prove that in Fig 7 and Fig 8 with various values of ε angle for some constant values of Re, Ha and S. As result that, it can see that in the convergent channel, the velocity rises with the ε angle, whereas it falls in the divergent channel. In Fig 9 and Fig 10, it is important to note that the behavior of the number Reynolds Re, which denotes the proximity of the inertia effect in comparison to an impact of viscosity. In the divergent case, the velocity distribution decreases with rising Re, and the convergent case, where it behaves oppositely. It is clear that the velocity profile increases as Re increases.

Table 2: Comparison between $\mathcal{BVP}4\mathrm{c}, \mathcal{DTM}, \mathcal{CDTM}, \mathcal{SDTM}, \mathcal{LDTM}$ and $\mathcal{GDTM}$ for $R_e = 15$, $S = 10$, $H = 100$ and $\varepsilon = 3^{\circ}$.

ξ	$\mathcal{BVP}4\mathrm{c}$	$\mathcal{DTM}$	$\mathcal{CDTM}$	$\mathcal{SDTM}$	$\mathcal{LDTM}$	$\mathcal{GDTM}$
0.0	1.00000000	1.00000000	1.00000000	1.000000000	1.00000000	1.00000000
0.1	0.990725861	0.990724328	0.990725844	0.990725861	0.990725863	0.990725774
0.2	0.962371821	0.9623656019	0.962371787	0.962371822	0.962371818	0.962371678
0.3	0.914292468	0.9142782997	0.914292422	0.914292471	0.914292461	0.914292293
0.4	0.846038007	0.8460125454	0.846037951	0.846038009	0.846038007	0.846037788
0.5	0.757326222	0.7572861240	0.757326161	0.757326223	0.757326228	0.757325981
0.6	0.647990091	0.6479323586	0.647990030	0.647990091	0.647990089	0.647989865
0.7	0.517900053	0.5178234271	0.517899999	0.517900053	0.517900043	0.517899858
0.8	0.366860237	0.3667697084	0.366860195	0.366860237	0.366860232	0.366860080
0.9	0.194477428	0.1943965110	0.194477403	0.194477427	0.194477427	0.194477338
1.0	0.00000000	0.00000000	0.00000000	0.00000000	0.00000000	0.00000000

Table 3: Comparison between $\mathcal{BVP4c}, \mathcal{DTM}, \mathcal{CDTM}, \mathcal{SDTM}, \mathcal{LDTM}$ and $\mathcal{GDTM}$ for $R_e = 25$, $S = 15$, $H = 500$, and $\varepsilon = 2^{\circ}$.

ξ	$\mathcal{BVP4c}$	$\mathcal{DTM}$	$\mathcal{CDTM}$	$\mathcal{SDTM}$	$\mathcal{LDTM}$	$\mathcal{GDTM}$
0.0	1.000000000	1.000000000	1.000000000	1.000000000	1.000000000	1.000000000
0.1	0.990884418	0.990882733	0.990884366	0.990884420	0.990884407	0.990884350
0.2	0.963001599	0.962994761	0.963001495	0.963001606	0.963001598	0.963001484
0.3	0.915670458	0.915654868	0.915670315	0.915670468	0.915670478	0.915670325
0.4	0.848362234	0.848334187	0.848362064	0.848362244	0.848362236	0.848362067
0.5	0.760665540	0.760621305	0.760665358	0.760665551	0.760665516	0.760665349
0.6	0.652225146	0.652161323	0.652224966	0.652225155	0.652225130	0.652224967
0.7	0.522652553	0.522567600	0.522652394	0.522652562	0.522652562	0.522652404
0.8	0.371406239	0.371305479	0.371406115	0.371406245	0.371406241	0.371406115
0.9	0.197638101	0.197547569	0.197638030	0.197638107	0.197638093	0.197638030
1.0	0.000000000	0.0000000000	0.0000000000	0.0000000000	0.0000000000	0.0000000000

Table 4: Comparison between $\mathcal{BVP4c}, \mathcal{DTM}, \mathcal{CDTM}, \mathcal{SDTM}, \mathcal{LDTM}$ and $\mathcal{GDTM}$ for $R_e = 20$, $S = 20$ $H = 150$, and $\varepsilon = 1^{\circ}$.

ξ	$\mathcal{BVP4c}$	$\mathcal{DTM}$	$\mathcal{CDTM}$	$\mathcal{SDTM}$	$\mathcal{LDTM}$	$\mathcal{GDTM}$
0.0	1.0000000000	1.0000000000	1.0000000000	1.0000000000	1.0000000000	1.0000000000
0.1	0.990618331	0.990618603	0.990618328	0.990618331	0.990618333	0.990618329
0.2	0.962092829	0.962093871	0.962092823	0.962092829	0.962092829	0.962092826
0.3	0.913929007	0.913931154	0.913929000	0.913929008	0.913929001	0.913929008
0.4	0.845729211	0.845732510	0.845729202	0.845729211	0.845729210	0.845729210
0.5	0.757178619	0.757182707	0.757178610	0.757178619	0.757178625	0.757178614
0.6	0.6480211648	0.648025177	0.648021155	0.648021164	0.648021166	0.648021161
0.7	0.518024835	0.518027452	0.518024826	0.518024835	0.518024830	0.518024834
0.8	0.366935910	0.366935802	0.366935904	0.366935910	0.366935908	0.366935908
0.9	0.194421566	0.194418860	0.194421562	0.194421566	0.194421567	0.194421564
1.0	0.00000000	0.00000000	0.00000000	0.00000000	0.00000000	0.00000000

Table 5: Comparison between $\mathcal{BVP4c}, \mathcal{DTM}, \mathcal{CDTM}, \mathcal{SDTM}, \mathcal{LDTM}$ and $\mathcal{GDTM}$ for $R_e = 15$, $S = 10 H = 50$, and $\varepsilon = -3^{\circ}$.

ξ	$\mathcal{BVP4c}$	$\mathcal{DTM}$	$\mathcal{CDTM}$	$\mathcal{SDTM}$	$\mathcal{LDTM}$	$\mathcal{GDTM}$
0.0	1.0000000000	1.0000000000	1.0000000000	1.0000000000	1.0000000000	1.0000000000
0.1	0.989567288	0.989566549	0.989567277	0.989567287	0.989567294	0.989567310
0.2	0.958807821	0.958804910	0.958807801	0.958807822	0.958807813	0.958807856
0.3	0.908261678	0.908255198	0.908261652	0.908261680	0.908261655	0.908261733
0.4	0.838159131	0.838147708	0.838159100	0.838159132	0.838159132	0.838159187
0.5	0.748487787	0.748470072	0.748487755	0.748487788	0.748487810	0.748487835
0.6	0.639070032	0.639044797	0.639070001	0.639070032	0.639070032	0.639070085
0.7	0.509652415	0.509619048	0.509652388	0.509652416	0.509652391	0.509652468
0.8	0.360008802	0.359969124	0.360008781	0.360008801	0.360008793	0.360008833
0.9	0.190058589	0.190022440	0.190058577	0.190058588	0.190058594	0.190058606
1.0	0.0000000000	0.0000000000	0.0000000000	0.0000000000	0.0000000000	0.0000000000

Table 6: Comparison between $\mathcal{BVP4c}, \mathcal{DTM}, \mathcal{CDTM}, \mathcal{SDTM}, \mathcal{LDTM}$ and $\mathcal{GDTM}$ for $R_e = 25$, $S = 20$ $H = 500$, and $\varepsilon = -1^{\circ}$.

ξ	$\mathcal{BVP4c}$	$\mathcal{DTM}$	$\mathcal{CDTM}$	$\mathcal{SDTM}$	$\mathcal{LDTM}$	$\mathcal{GDTM}$
0.0	1.0000000000	1.000000000	1.000000000	1.000000000	1.0000000000	1.0000000000
0.1	0.989656178	0.989656707	0.989656174	0.989656177	0.989656174	0.989656163
0.2	0.958994465	0.958996504	0.958994459	0.958994465	0.958994462	0.958994439
0.3	0.908409561	0.908413884	0.908409554	0.908409561	0.908409563	0.908409538
0.4	0.838105992	0.838113062	0.838105984	0.838105992	0.838105993	0.838105961
0.5	0.748132841	0.748142697	0.748132833	0.748132841	0.748132839	0.748132802
0.6	0.638425667	0.638437800	0.638425658	0.638425667	0.638425664	0.638425635
0.7	0.508856022	0.508869235	0.508856015	0.508856022	0.508856022	0.508856000
0.8	0.359289154	0.359301378	0.359289148	0.359289154	0.359289154	0.359289131
0.9	0.189650336	0.189658472	0.189650332	0.189650336	0.189650335	0.189650323
1.0	0.0000000000	0.00000000000	0.0000000000	0.0000000000	0.0000000000	0.0000000000

Table 7: **Comparison between $\mathcal{BVP4c}, \mathcal{DTM}, \mathcal{CDTM}, \mathcal{SDTM}, \mathcal{LDTM}$ and $\mathcal{GDTM}$ for $R_e = 20$, $H = 250, S = 15$ and $\varepsilon = -2^{\circ}$.**

ξ	$\mathcal{BVP4c}$	$\mathcal{DTM}$	$\mathcal{CDTM}$	$\mathcal{SDTM}$	$\mathcal{LDTM}$	$\mathcal{GDTM}$
0.0	1.0000000	1.0000000	1.0000000	1.0000000	1.0000000	1.0000000
0.1	0.989606383	0.989607651	0.989606368	0.989606381	0.989606386	0.989606473
0.2	0.958959829	0.958964596	0.958959803	0.958959830	0.958959826	0.958959967
0.3	0.908593093	0.908602789	0.908593059	0.908593095	0.908593078	0.908593297
0.4	0.838724573	0.838739417	0.838724534	0.838724575	0.838724568	0.838724792
0.5	0.749319506	0.749338106	0.749319466	0.749319508	0.749319516	0.749319705
0.6	0.640159618	0.640178660	0.640159580	0.640159620	0.640159621	0.640159824
0.7	0.510922879	0.510937224	0.510922845	0.510922881	0.510922869	0.510923077
0.8	0.361275318	0.361279426	0.361275293	0.361275319	0.361275312	0.361275448
0.9	0.190976577	0.190969639	0.190976562	0.190976577	0.190976577	0.190976648
1.0	0.000000000	0.000000000	0.000000000	0.0000000000	0.0000000000	0.0000000000

Table 8: **Comparison between the error $\mathcal{BVP4c}, \mathcal{DTM}, \mathcal{CDTM}, \mathcal{SDTM}, \mathcal{LDTM}$ and $\mathcal{GDTM}$for $R_e = 30$, $H = 400, S = 15$ and $\varepsilon = 1^{\circ}$.**

ξ	$\mathcal{DTM}$	$\mathcal{CDTM}$	$\mathcal{SDTM}$	$\mathcal{LDTM}$	$\mathcal{GDTM}$
0.0	0.0000000	0.0000000	0.0000000	0.0000000	0.0000000
0.1	3.25×10^{-7}	2.01×10^{-10}	9.08×10^{-10}	4.03×10^{-9}	1.96×10^{-8}
0.2	1.34×10^{-6}	1.24×10^{-9}	1.04×10^{-9}	5.20×10^{-10}	2.30×10^{-8}
0.3	3.21×10^{-6}	1.97×10^{-9}	1.31×10^{-9}	6.58×10^{-9}	5.12×10^{-8}
0.4	6.21×10^{-6}	1.78×10^{-9}	2.49×10^{-9}	2.37×10^{-10}	6.42×10^{-8}
0.5	1.09×10^{-5}	2.13×10^{-9}	3.19×10^{-9}	1.10×10^{-8}	5.67×10^{-8}
0.6	1.82×10^{-5}	1.24×10^{-9}	4.37×10^{-9}	8.12×10^{-9}	6.65×10^{-8}
0.7	3.01×10^{-5}	1.17×10^{-9}	5.29×10^{-9}	4.31×10^{-9}	9.15×10^{-8}
0.8	4.97×10^{-5}	2.77×10^{-9}	6.11×10^{-9}	1.01×10^{-9}	8.47×10^{-8}
0.9	8.28×10^{-5}	2.63×10^{-10}	1.05×10^{-8}	1.73×10^{-8}	8.05×10^{-8}
1.0	0.000000000	0.000000000	0.000000000	0.000000000	0.000000000

Table 9: **Comparison between the error $\mathcal{BVP4c}, \mathcal{DTM}, \mathcal{CDTM}, \mathcal{SDTM}, \mathcal{LDTM}$ and $\mathcal{GDTM}$ for $R_e = 25$, $H = 200, S = 10$ and $\varepsilon = 3^{\circ}$.**

ξ	$\mathcal{DTM}$	$\mathcal{CDTM}$	$\mathcal{SDTM}$	$\mathcal{LDTM}$	$\mathcal{GDTM}$
0.0	0.0000000	0.0000000	0.0000000	0.0000000	0.0000000
0.1	4.68×10^{-6}	4.94×10^{-9}	2.52×10^{-9}	7.57×10^{-10}	1.61×10^{-8}
0.2	1.95×10^{-5}	1.03×10^{-8}	7.80×10^{-9}	4.16×10^{-9}	2.60×10^{-8}
0.3	4.68×10^{-5}	1.46×10^{-8}	1.20×10^{-8}	1.74×10^{-8}	3.58×10^{-8}
0.4	9.09×10^{-5}	1.82×10^{-8}	1.58×10^{-8}	4.52×10^{-9}	4.95×10^{-8}
0.5	1.59×10^{-4}	2.08×10^{-8}	2.02×10^{-8}	1.80×10^{-8}	6.00×10^{-8}
0.6	2.68×10^{-4}	2.30×10^{-8}	2.38×10^{-8}	6.26×10^{-9}	6.61×10^{-8}
0.7	4.44×10^{-4}	2.52×10^{-8}	2.67×10^{-8}	2.52×10^{-8}	7.34×10^{-8}
0.8	7.36×10^{-4}	2.68×10^{-8}	2.79×10^{-8}	1.70×10^{-8}	8.38×10^{-8}
0.9	1.22×10^{-3}	3.01×10^{-8}	2.48×10^{-8}	1.27×10^{-8}	8.99×10^{-8}
1.0	0.0000000	0.0000000	0.0000000	0.0000000	0.0000000

Table 10: **Comparison between the error $\mathcal{BVP4c}, \mathcal{DTM}, \mathcal{CDTM}, \mathcal{SDTM}, \mathcal{LDTM}$ and $\mathcal{GDTM}$ for $R_e = 15$, $H = 500, S = 30$ and $\varepsilon = -3^{\circ}$.**

ξ	$\mathcal{DTM}$	$\mathcal{CDTM}$	$\mathcal{SDTM}$	$\mathcal{LDTM}$	$\mathcal{GDTM}$
0.0	0.0000000	0.0000000	0.0000000	0.0000000	0.0000000
0.1	5.23×10^{-5}	6.43×10^{-8}	2.02×10^{-9}	1.25×10^{-8}	1.97×10^{-8}
0.2	2.08×10^{-4}	1.23×10^{-7}	9.86×10^{-9}	1.04×10^{-9}	4.34×10^{-8}
0.3	4.77×10^{-4}	1.64×10^{-7}	1.60×10^{-8}	2.30×10^{-8}	3.68×10^{-8}
0.4	8.98×10^{-4}	1.99×10^{-7}	1.82×10^{-8}	5.34×10^{-9}	4.66×10^{-8}
0.5	1.53×10^{-3}	2.25×10^{-7}	2.10×10^{-8}	4.60×10^{-8}	7.06×10^{-8}
0.6	2.51×10^{-3}	2.47×10^{-7}	2.32×10^{-8}	2.79×10^{-8}	7.19×10^{-8}
0.7	4.08×10^{-3}	2.63×10^{-7}	2.66×10^{-8}	2.48×10^{-8}	5.71×10^{-8}
0.8	6.68×10^{-3}	2.72×10^{-7}	3.44×10^{-8}	9.25×10^{-9}	7.05×10^{-8}
0.9	1.11×10^{-3}	2.82×10^{-7}	4.89×10^{-8}	5.33×10^{-8}	7.86×10^{-8}
1.0	0.00000000	0.00000000	0.00000000	0.00000000	0.00000000

Table 11: Comparison between the error $\mathcal{BVP4c}, \mathcal{DTM}, \mathcal{CDTM}, \mathcal{SDTM}, \mathcal{LDTM}$ and $\mathcal{GDTM}$ For $R_e = 20$, $H = 300, S = 25$ and $\varepsilon = -1^{\circ}$.

ξ	$\mathcal{DTM}$	$\mathcal{CDTM}$	$\mathcal{SDTM}$	$\mathcal{LDTM}$	$\mathcal{GDTM}$
0.0	0.0000000	0.0000000	0.0000000	0.0000000	0.0000000
0.1	1.18×10^{-4}	8.08×10^{-10}	5.05×10^{-10}	6.26×10^{-9}	1.61×10^{-8}
0.2	4.66×10^{-4}	8.35×10^{-10}	2.08×10^{-10}	1.04×10^{-10}	2.60×10^{-8}
0.3	1.02×10^{-3}	9.94×10^{-10}	2.20×10^{-10}	1.23×10^{-8}	3.58×10^{-8}
0.4	1.77×10^{-3}	1.44×10^{-9}	4.80×10^{-10}	2.40×10^{-10}	4.95×10^{-8}
0.5	2.69×10^{-3}	1.88×10^{-9}	8.08×10^{-10}	1.82×10^{-8}	6.00×10^{-8}
0.6	3.70×10^{-3}	2.21×10^{-9}	1.10×10^{-10}	8.55×10^{-9}	6.61×10^{-8}
0.7	4.86×10^{-3}	2.19×10^{-9}	9.97×10^{-10}	1.55×10^{-8}	7.34×10^{-8}
0.8	6.04×10^{-3}	3.12×10^{-9}	1.13×10^{-9}	7.94×10^{-9}	8.38×10^{-8}
0.9	7.22×10^{-3}	3.77×10^{-9}	2.69×10^{-9}	1.99×10^{-8}	8.99×10^{-8}
1.0	0.0000000	0.0000000	0.0000000	0.0000000	0.0000000

Table 12: The convergence of values Π .

Approximate Order	$R_e = 10$, $S = 0$, $H_a = 100$ $\varepsilon = 1^{\circ}$	$\varepsilon = -1^{\circ}$	$R_e = 20$, $S = 10$, $H_a = 250$ $\varepsilon = 3^{\circ}$	$\varepsilon = -3^{\circ}$
Order15	-1.020983218	-0.9747006257	-1.715275705	-0.9796786038
Order16	-1.020983218	-0.9747006257	-1.836816580	-0.9795422259
Order17	-1.020983223	-0.9747006257	-1.900702406	-0.9796325464
Order18	-1.020983223	-0.9747006295	-1.966734487	-0.9795737763
Order19	-1.020983222	-0.9747006295	-2.034963996	-0.9795954808
Order 20	-1.020983222	-0.9747006294	-2.105441316	-0.9795911523
Order 21	-1.020983222	-0.9747006294	-2.178216074	-0.9795911393
Order 22	-1.020983222	-0.9747006294	-2.253337384	-0.9795922592
Order 23	-1.020983222	-0.9747006294	-1.020983222	-0.9795915917
Order 24	-1.020983222	-0.9747006294	-1.020983222	-0.9795918737

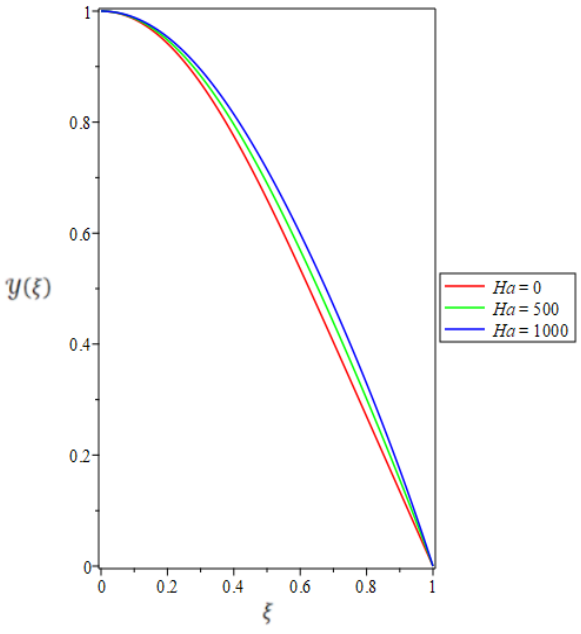

FIGURE 3. Velocity distribution for different Ha diverging for $Re = 100, S = 20$ and $\varepsilon = 3°$

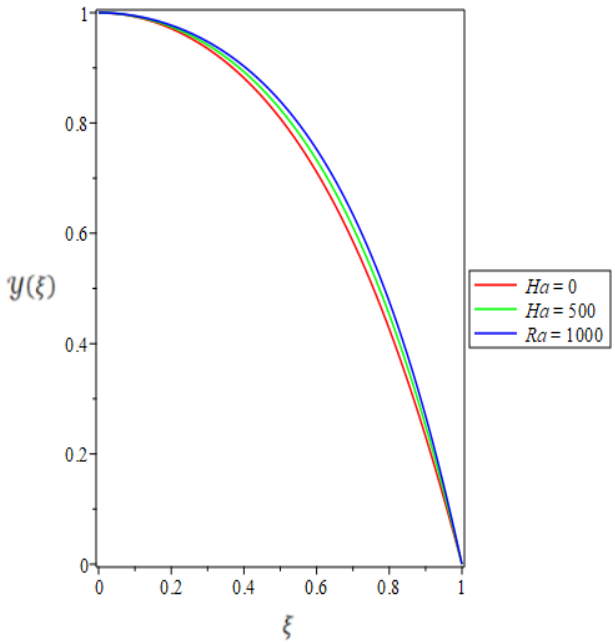

FIGURE 4. Velocity distribution for different Ha in converging for $Re = 100, S = 20$ and $\varepsilon = -3°$.

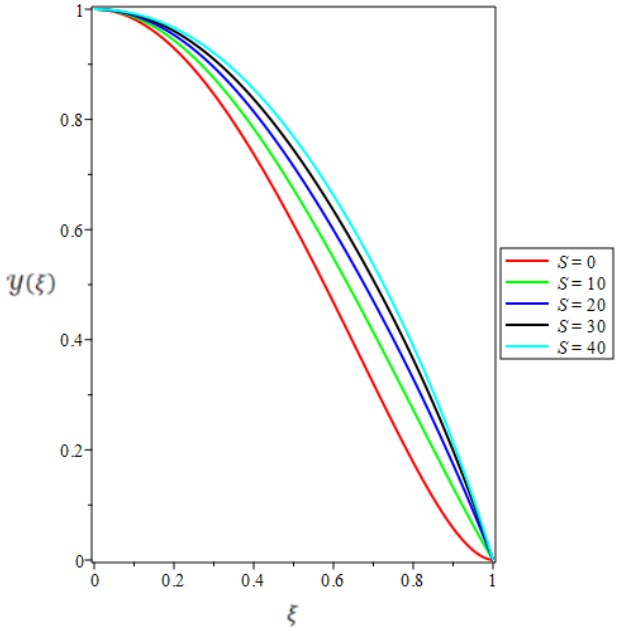

FIGURE5. Velocity distribution for different S in diverge for $Re = 20, Ha = 1000$ and ε = 3 °.

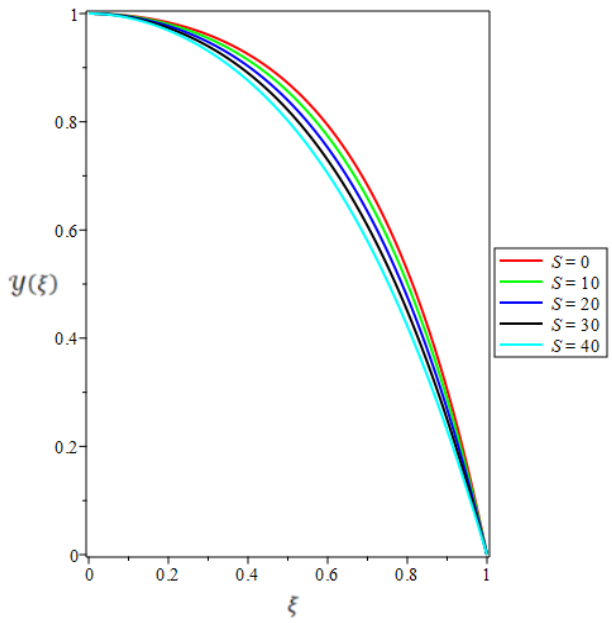

FIGURE6: Velocity distribution for different S in converge for $Re = 20, Ha = 1000$ and ε = 3°.

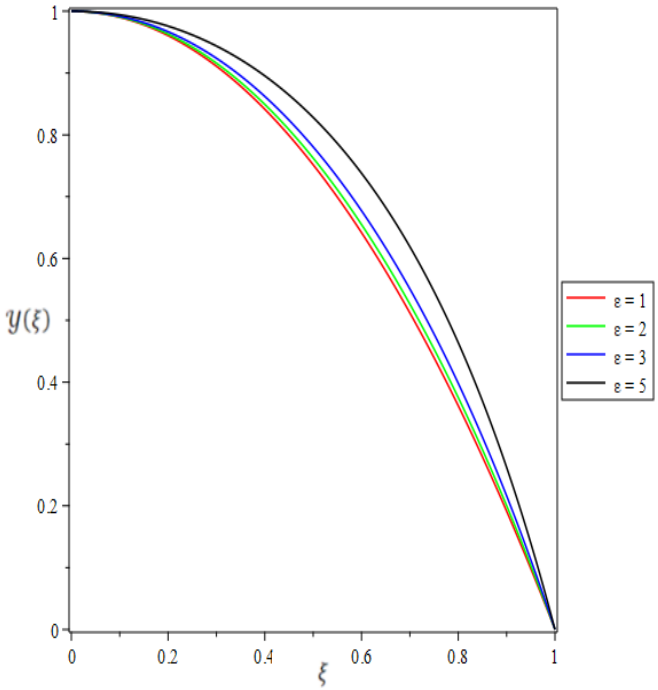

FIGURE 7. Velocity distribution for different ε in diverging for $Re = 50, S = 20$ and $Ha = 1000$.

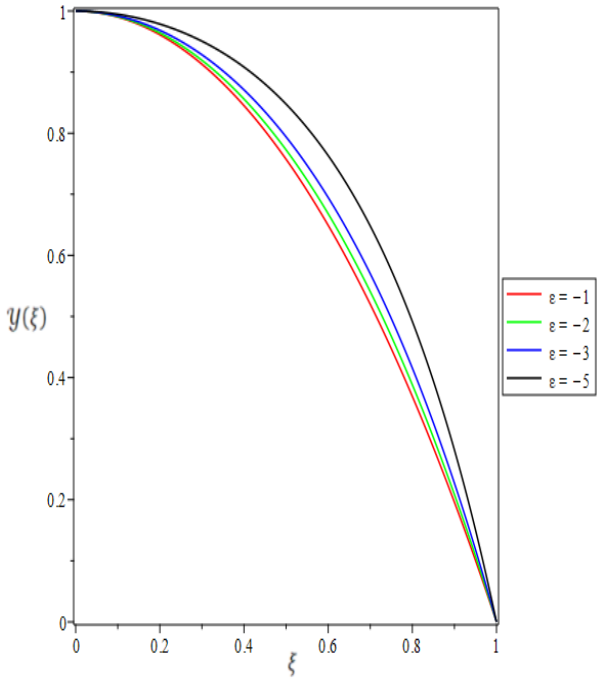

FIGURE 8. Velocity distribution for different ε in converging for $Re = 50, S = 20$ and $Ha = 1000$.

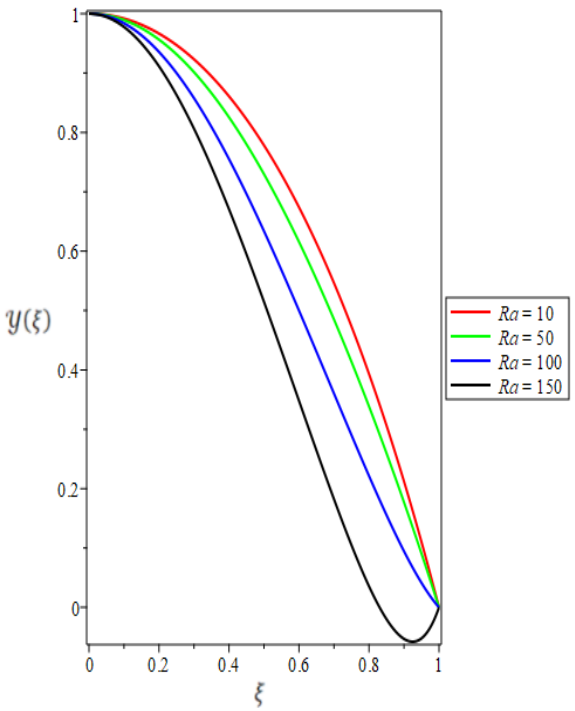

FIGURE 9. Velocity distribution for different Re in diverging for $Ha = 1000, S = 20$ and $\varepsilon = 3°$.

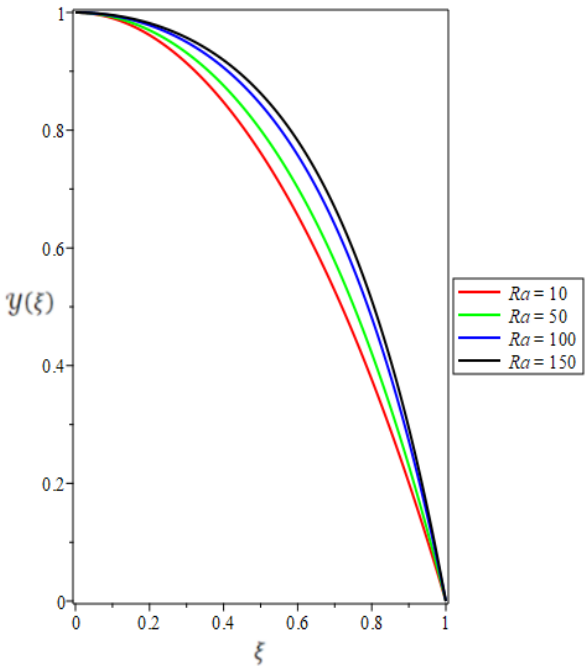

FIGURE 10. Velocity distribution for different Re in converging $Ha = 1000, S = 20$ and $\varepsilon = -3°$.

8. CONCLUSIONS

In this paper, A third-order magnetic-hydrodynamic Jeffrey Hamel flow with suction-injection has been resolved numerically and analytically. The comparison demonstrates that the proportion of errors related with the $\mathcal{ODTM}$ is much lower than that related to $\mathcal{DTM}$. Based on our analysis, it can be inferred that the $\mathcal{ODTM}$ exhibits more accuracy compared to the differential transform method. The examination shows that the $\mathcal{ODTM}$ has a substantially reduced proportion of mistakes compared to $\mathcal{DTM}$. Our research suggests that, when contrasted with the differential transform method, $\mathcal{ODTM}$ is more precise. Since $\mathcal{DTM}$ and $\mathcal{ODTM}$ does not require any parameters, linearization, discretization, or minor perturbations, it can be utilized to solve a variety of non-linear ordinary differential equations and have been successful in doing so. It can be seen that there is excellent agreement with numerical findings. Also, it is a potent way for solving in high magnetic field MHD Jeffery-Hamel flow. The main out coming of this investigation can be listed as:

- As Reynolds numbers rise, an unfavorable pressure gradient results, which lowers velocity close to the walls. And in the event of a convergent channel, the opposite behavior.
- Both divergent and convergent channels will experience rising velocity as the Hartmann number increases.
- It is because the vertical velocity in the divergent channel has a radial velocity in the same direction of fluid flow and behaves in the opposite way in the case of the convergent one that changing the suction-injection parameter permits the velocity to increase for divergent channels and has the opposite effect in the case of convergent channels. he general conclusions of this study can be explain in Fig 11 and Fig 12 as follows:

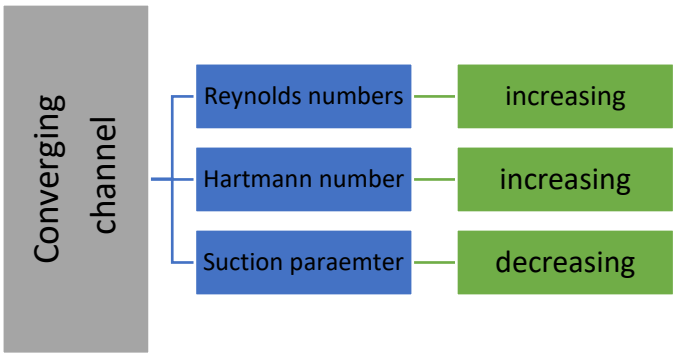

FIGURE 11. The behavior of the velocity for convergent channel.

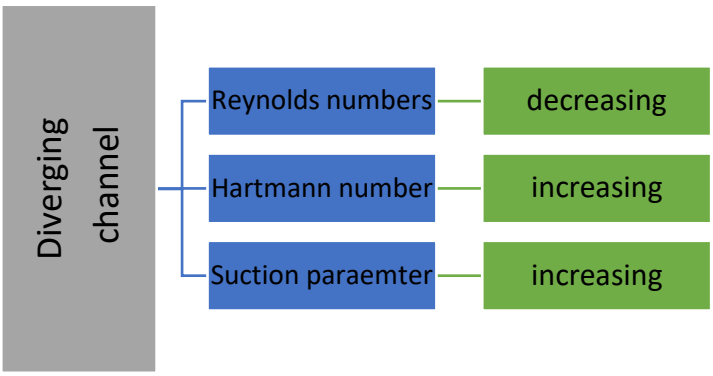

FIGURE 12. The behavior of the velocity for divergent channel.

REFERENCES

[1] G. B. Jeffery, "L. The two-dimensional steady motion of a viscous fluid," Lond. Edinb. Dublin Philos. Mag. J. Sci., vol. 29, no. 172, pp. 455–465, 1915.

[2] W. Adel, K. E. Biçer, and M. Sezer, "A novel numerical approach for simulating the nonlinear MHD Jeffery–Hamel flow problem," Int. J. Appl. Comput. Math., vol. 7, no. 3, 2021.

[3] E. Richard Onyango, M. Ngugi Kinyanjui, M. Kimathi, and S. Mohan Uppal, "Heat and mass transfer on MHD Jeffrey-Hamel flow in presence of inclined magnetic field," Appl. Comput. Math., vol. 9, no. 4, p. 108, 2020.

[4] A. J. Majeed and A. Z. J. A. Nabi, "Three iterative methods for solving Jeffery-Hamel flow problem," Kuwait Journal of Science, vol. 1, 2020.

[5] S. Rehman, Hashim, Y. Trabelsi, S. Alqahtani, S. Alshehery, and S. M. Eldin, "A renovated Jaffrey-Hamel flow problem and new scaling statistics for heat, mass fluxes with Cattaneo–Christov heat flux model," Case Stud. Therm. Eng., vol. 43, no. 102787, p. 102787, 2023.

[6] M. I. Khan and F. Alzahrani, "Nonlinear dissipative slip flow of Jeffrey nanomaterial towards a curved surface with entropy generation and activation energy," Math. Comput. Simul., vol. 185, pp. 47–61, 2021.

[7] F. Mebarek-Oudina and O. D. Makinde, "Numerical simulation of oscillatory MHD natural convection in cylindrical annulus: Prandtl number effect," Defect Diffus. For., vol. 387, pp. 417–427, 2018.

[8] J. Reza, F. Mebarek-Oudina, and O. D. Makinde, "MHD slip flow of cu-Kerosene nanofluid in a channel with stretching walls using 3-stage Lobatto IIIA formula," Defect Diffus. For., vol. 387, pp. 51–62, 2018.

[9] A. M. Jasim, "Study of the impact of unsteady squeezing magnetohydrodynamics Copper-water with injection-suction on nanofluid flow between two parallel plates in porous medium," Iraqi J. Sci., pp. 3909–3924, 2022.

[10] J. Raza, F. Mebarek-Oudina, and A. J. Chamkha, "Magnetohydrodynamic flow of molybdenum disulfide nanofluid in a channel with shape effects," Multidiscip. Model. Mater. Struct., vol. 15, no. 4, pp. 737–757, 2019.

[11] Z. Asghar, R. S. Saif, and N. Ali, "Investigation of boundary stresses on MHD flow in a convergent/divergent channel: An analytical and numerical study," Alex. Eng. J., vol. 61, no. 6, pp. 4479–4490, 2022.

[12] S. Dinarvand, H. Berrehal, I. Pop, and A. J. Chamkha, "Blood-based hybrid nanofluid flow through converging/diverging channel with multiple slips effect: a development of Jeffery-Hamel problem," Int. J. Numer. Methods Heat Fluid Flow, vol. 33, no. 3, pp. 1144–1160, 2023.

[13] S. Nadeem, N. S. Akbar, T. Hayat, and A. A. Hendi, "Influence of heat and mass transfer on Newtonian biomagnetic fluid of blood flow through a tapered porous arteries with a stenosis," Transp. Porous Media, vol. 91, no. 1, pp. 81–100, 2012.

[14] M. Chutia, "Effect of variable thermal conductivity and the inclined magnetic field on MHD plane poiseuille flow in a Porous channel with non-uniform plate temperature," Journal of Computational & Applied Research in Mechanical Engineering (JCARME), vol. 8, no. 1, pp. 75–84, 2018.

[15] A. M. Jasim, "Exploration of no-slip and slip of unsteady squeezing flow fluid through a derivatives series algorithm," Adv. Res. Fluid Mech. Therm. Sci., vol. 100, no. 1, pp. 11–29, 2022.

[16] A. M. Jasim, "Study effect of MHD on squeezing flow of water-based Casson nanofluid in a porous medium between two parallel plates," in THE SECOND INTERNATIONAL SCIENTIFIC CONFERENCE (SISC2021): College of Science, Al-Nahrain University, 2023.

[17] M. Saqib, I. Khan, and S. Shafie, "Natural convection channel flow of CMC-based CNTs nanofluid," Eur. Phys. J. Plus, vol. 133, no. 12, 2018.

[18] M. Saqib, I. Khan, and S. Shafie, "Application of fractional differential equations to heat transfer in hybrid nanofluid: modeling and solution via integral transforms," Adv. Differ. Equ., vol. 2019, no. 1, 2019.

[19] F. Mebarek-Oudina, "Numerical modeling of the hydrodynamic stability in vertical annulus with heat source of different lengths," Eng. Sci. Technol. Int. J., vol. 20, no. 4, pp. 1324–1333, 2017.

[20] J. Raza, F. Mebarek-Oudina, and B. Mahanthesh, "Magnetohydrodynamic flow of nano Williamson fluid generated by stretching plate with multiple slips," Multidiscip. Model. Mater. Struct., vol. 15, no. 5, pp. 871–894, 2019.

[21] B. Mahanthesh, B. J. Gireesha, N. S. Shashikumar, T. Hayat, and A. Alsaedi, "Marangoni convection in Casson liquid flow due to an infinite disk with exponential space dependent heat source and cross-diffusion effects," Results Phys., vol. 9, pp. 78–85, 2018.

[22] B. J. Gireesha, P. B. S. Kumar, B. Mahanthesh, S. A. Shehzad, and F. M. Abbasi, "Nonlinear gravitational and radiation aspects in nanoliquid with exponential space dependent heat source and variable viscosity," Microgravity Sci. Technol., vol. 30, no. 3, pp. 257–264, 2018.

[23] M. Gudekote, R. Choudhari, H. Vaidya, and K. V. Prasad, "Peristaltic flow of Herschel-Bulkley fluid in an elastic tube with slip at porous walls," Journal of Advanced Research in Fluid Mechanics and Thermal Sciences, vol. 52, no. 1, pp. 63–75, 2018.

[24] M. Usman, M. Hamid, U. Khan, S. T. Mohyud Din, M. A. Iqbal, and W. Wang, "Differential transform method for unsteady nanofluid flow and heat transfer," Alex. Eng. J., vol. 57, no. 3, pp. 1867–1875, 2018.

[25] B. Kundu, R. Das, and K.-S. Lee, "Differential transform method for thermal analysis of exponential fins under sensible and latent heat transfer," Procedia Eng., vol. 127, pp. 287–294, 2015.

[26] M. A. Rasheed and S. N. Kadhim, "Numerical solutions of two-dimensional vorticity transport equation using Crank-Nicolson method," Baghdad Sci. J., vol. 19, no. 2, p. 0321, 2022.

[27] N. J. Noon, "Numerical analysis of least-squares group finite element method for coupled Burgers' problem," Baghdad Sci. J., vol. 18, no. 4(Suppl.), p. 1521, 2021.

[28] W. S. Ali and H. S. Ali, "Numerical solution for linear state space systems using Haar wavelets method," Baghdad Sci. J., vol. 19, no. 1, p. 0084, 2022

[29] S. Sepasgozar, M. Faraji, and P. Valipour, "Application of differential transformation method (DTM) for heat and mass transfer in a porous channel," Propuls. Power Res., vol. 6, no. 1, pp. 41–48, 2017.

[30] N. D. Patel and R. Meher, "Differential transform method for solving for fingero-imbibition phenomena arising in double phase flow through homogeneous porous media," Mathematical Sciences, IMRF Journals, vol. 6, no. 1, pp. 1–5, 2017.

[31] M. M. Rashidi, A. Muhammad, R. Behnam, T. R. Mohammad, and B. Sumra, "Mixed convection boundary layer flow of a micro polar fluid towards a heated shrinking sheet by homotopy analysis method," Thermal Science, vol. 20, pp. 21–34, 2016.

[32] H. Salim, M. Fateh, and R. S. Mohamed, "Analysis of MHD Jeffery Hamel flow with suction-injection by homotopy analysis method," Journal of Advanced Research in Fluid Mechanics and Thermal Sciences, vol. 58, no. 2, pp. 173–186, 2019.

[33] R. Meher and N. D. Patel, "Analytical Investigation of MHD Jeffery–Hamel flow problem with heat transfer by differential transform method," SN Appl. Sci., vol. 1, no. 7, 2019.

[34] N. D. Patel and M. Ramakanta, "Analytical investigation of Jeffery-Hemal flow with magnetic field by differential transform method," Int. J. Adv. Appl. Math, vol. 6, no. 1, pp. 1–9, 2018.

[35] Al-Hachami, A. K. (2019), Magnetic Reconnection in the Absence of Three-Dimension Null Point. Herald of the Bauman Mosco state Technical University. (6), 50-66